Topics in Catalysis
https://doi.org/10.1007/s11244-024-01924-w

ORIGINAL PAPER

Influence of Doping of Niobium Oxide on the Catalytic Activity of Pt/Al_2O_3 for CO Oxidation

Le Yu[1,2] · Yejin Song[2] · Seunghwa Hong[2] · Zhaoyi Xu[1] · Shourong Zheng[1] · Jeong Young Park[2]

Accepted: 19 February 2024

Abstract

Pt-based alumina catalysts doped with varying niobium contents (i.e., 0, 1.20, 2.84, and 4.73 wt%, denoted as Pt/Nb–Al_2O_3) were synthesized via stepwise impregnation for catalytic CO oxidation. The effective incorporation of Nb species without altering the fundamental properties of the Al_2O_3 support was confirmed by the characterization using XRD, Raman, and TEM. Pt metallic particles were uniformly deposited on the niobium-doped alumina (Nb–Al_2O_3) support. H_2-TPR and CO–TPD analyses were performed to reveal the influence of niobium doping on catalyst reduction and CO adsorption properties. The results consistently demonstrate that the doping of niobium affects reducibility and alleviates the competitive adsorption between CO and O_2 during the CO reaction. Particularly, when compared to both undoped and excessively doped Pt/Al_2O_3 catalysts, the catalyst featuring a 2.84 wt% Nb content on $Pt_{1.4}/Nb_{2.8}$–Al_2O_3 displayed the most promising catalytic performance, with a turnover frequency of 3.12 s^{-1} at 180 °C. This superior performance can be attributed to electron transfer at the Pt/NbOx interface.

Keywords Nb doping · Pt-based catalyst · CO oxidation

1 Introduction

Catalytic oxidation of carbon monoxide (CO) not only plays a critical role in heterogeneous catalysis as a classic model reaction but also shows major practical potential in automotive catalysts, air cleaners, and gas mask applications, as it is an effective method for toxic CO gas removal [1–3]. Research on catalytic CO oxidation has gained increasing attention in recent years, with a particular focus on noble metal platinum group catalysts [4–9]. Noble metal platinum (Pt) species serve as active sites in the adsorption of CO during CO oxidation reaction. CO molecules are strongly adsorbed on the Pt atoms through the Langmuir–Hinshelwood mechanism and subsequently combined with the surface oxygen atom to form carbon dioxide (CO_2), which has been clarified as the crucial rate-determining step of the CO oxidation reaction [10, 11]. Nevertheless, the excessive adsorbed CO can hinder the O_2 adsorption and activation to some extent, resulting in an effect known as CO poisoning, which leads to reduced catalytic efficiency [12–14].

To solve the CO poisoning on Pt-based catalysts, a large amount of research work has been devoted to using metal–support interaction in the past decade. It has been established that metal–oxide interactions can greatly impact the properties of noble metals (such as dispersion, particle size distribution, valence state, and thermal stability), thereby affecting catalytic performance [15, 16]. For instance, Song et al. investigated Pt supported on CeO_2 catalysts modified with transition metal oxides and applied it to CO oxidation. They demonstrated that the electron-deficient Pt, due to the strong interaction between Pt and doping metal oxide, exhibited weaker CO adsorption strength [17]. Similarly, Tran et al. indicated that the dopants could enhance the interaction between the Pt nanoparticles and the catalyst support for iron-doped ZnO, resulting in improved catalytic activity [18]. Therefore, the introduction of transition metal

✉ Shourong Zheng
srzheng@nju.edu.cn

✉ Jeong Young Park
jeongypark@kaist.ac.kr

[1] State Key Laboratory of Pollution Control and Resource Reuse, School of the Environment, Nanjing University, Nanjing 210023, People's Republic of China

[2] Department of Chemistry, Korea Advanced Institute of Science and Technology (KAIST), Daejeon 34141, Republic of Korea

Published online: 29 March 2024

oxides into Pt-based catalysts could be a feasible strategy to improve the catalytic oxidation of CO.

Niobium oxides (NbO_x) are used widely in catalysis and in electrochromic and photoelectrochemical devices, due to the variable electrical conductivity, refractive index, and photoelectric properties produced by different structures [19, 20]. It is reported that the use of niobium oxides (Nb_2O_5) as a support can control oxygen vacancies by regulating the calcination atmosphere and time, which promotes the catalytic activity of CO oxidation, while oxygen activation on oxygen vacancy is more efficient for Pt/Nb_2O_5 catalysts [21]. In addition, Nb-based material is also widely applied as a solid acid catalyst. Zhang et al. proposed that Nb doping increased acid sites and weakened CO−Cu^+ bond strength for CuO_x/CeO_2 catalysts [22]. Jardim et al. studied the preferential oxidation of CO in excess of H_2 on $Pt/CeO_2–Nb_2O_5$ catalysts and concluded that the presence of Nb in the supports inhibited their ability to adsorb CO [23].

Based on the above considerations, we fabricated a Pt-based catalyst on an Al_2O_3 support doped with NbO_x, and $Pt/Nb–Al_2O_3$ was synthesized by a stepwise impregnation method. This study also compared the catalytic performance between Pt/Al_2O_3 with different transition metal oxide dopants. Combining a series of characterization and CO catalytic oxidation performance of $Pt/Nb–Al_2O_3$ with varying NbO_x amounts would explore the influence of doping of NbO_x on the physical and chemical properties of Pt/Al_2O_3 catalyst and the catalytic oxidation activity of CO.

2 Materials and Methods

2.1 Materials

Ammonium niobate(V) oxalate hydrate ($Nb(HC_2O_4)_5{\cdot}nH_2O$, 99.99%), Ammonium vanadate (NH_4VO_3, 99.0%), Ammonium metatungstate hydrate ($(NH_4)_6W_{12}O_{39}{\cdot}xH_2O$, ≥ 85.0%), chloroplatinic acid hexahydrate ($H_2PtCl_6{\cdot}6H_2O$, 99.99%), and aluminum oxide (Al_2O_3, 99%) were purchased from Sigma-Aldrich. Ammonium molybdate $4H_2O$ ($(NH_4)_6Mo_7O_{24}{\cdot}4H_2O$, extra pure, > 98.0%) was purchased from Daejung Chemicals & Metals Co., Ltd. To eliminate trace metals and impurities, commercial Al_2O_3 was carefully pretreated with a high-temperature calcination under 600 °C for 4 h. Unless otherwise specified, all chemicals are analytically pure.

2.2 Catalyst Preparation

2.2.1 Nb-Doped Al_2O_3 Carrier

Pretreated Al_2O_3 and $Nb(HC_2O_4)_5{\cdot}nH_2O$ were dissolved in 40 mL of deionized water and stirred in a water bath at 40 °C for 16 h, then the water was evaporated at 90 °C; subsequently, the dried powder was placed in a muffle furnace for 4 h at 450 °C, which aimed to remove impurity ions by high-temperature treatment to obtain Nb-doped Al_2O_3 carrier $Nb–Al_2O_3$. The Nb precursor dosage was changed to acquire a catalyst with various dopant amounts; Nb doping amounts were determined to be 1.20, 2.84, and 4.73 wt% using an inductively coupled plasma optical emission spectrometer (ICP-OES).

2.2.2 Nb-Doped Pt/Al_2O_3 Catalyst

Pt-based niobium alumina material was synthesized using the traditional wet-impregnation method. In brief, the as-prepared $Nb–Al_2O_3$ was dispersed in an aqueous solution containing hydrochloric acid, which was stirred for 4 h under ambient conditions. 265 mg of Pt precursor $H_2PtCl_6{\cdot}6H_2O$ was used with 1.0 g of $Nb–Al_2O_3$ carrier powder, targeting a Pt loading of 1.0 wt%. The dry powder was transferred to a muffle furnace for 300 °C calcination, which was held for 4 h, and the high-temperature treatment tightly combined the platinum oxide and $Nb–Al_2O_3$. Finally, it was exposed to high-temperature reduction treatment in a hydrogen atmosphere, calcination at 200 °C in 3.9% H_2/Ar for 2 h, and cooled down to room temperature to obtain a dark gray powder, which is the Nb-doped Pt/Al_2O_3 catalyst $Pt/Nb–Al_2O_3$. The real Pt loading and Nb doping amounts were determined to be 1.20 wt% and 4.73 wt% (seen in Table 1), respectively. For comparison, we prepared other transition metals as dopants utilizing a similar process as $Pt/Nb–Al_2O_3$, named with $Pt/M–Al_2O_3$ [M = vanadium (V), molybdenum (Mo), and tungsten (W)]. Similarly, Pt/Al_2O_3 without dopant was also prepared by wet impregnation.

Table 1 Characterization and catalytic activity of the Pt/Al_2O_3 and $Pt/Nb–Al_2O_3$ catalysts

Catalysts	Pt content[a] (wt%)	Nb content[a] (wt%)	Pt particle size[b](nm)	TOF (S^{-1})	Ea (kcal/mol)
$Pt_{1.1}/Al_2O_3$	1.07	–[c]	1.31	2.27	21.40
$Pt_{1.0}/Nb_{1.2}–Al_2O_3$	1.00	1.20	1.84	2.71	18.64
$Pt_{1.4}/Nb_{2.8}–Al_2O_3$	1.35	2.84	1.39	3.12	15.25
$Pt_{1.2}/Nb_{4.7}–Al_2O_3$	1.20	4.73	1.95	2.74	16.00

[a]Determined by ICP-OES

[b]Calculated on the basis of TEM images

[c]Not detected

2.3 Characterization of the Catalysts

The size and morphology of the synthesized catalysts were assessed by transmission electron microscopy (TEM, Thermo Fisher, Talos F200X operated at 200 kV) accompanied by energy dispersive X-ray spectroscopy (EDS). The amount of Nb and Pt loading was measured by ICP-OES using a Thermal Scientific iCAP 6300. X-ray diffraction (XRD) patterns of the samples were recorded using a High-Resolution powder X-ray diffractometer (Rigaku, Smartlab at 45 kV and 200 mA) that scanned 2θ values between 10° and 80°. More structural characterization was obtained by the Raman spectroscopy technique employing LabRAM HR Evolution (Horiba, Japan) with a 514 nm laser source. X-ray photoelectron spectroscopy (XPS) was utilized to examine the chemical states of metal species on samples (Thermo VG Scientific, Sigma Probe). Binding energy calibration was based on C1s at 284.6 eV. XPSPeak 41 software was used for fitting the XPS peaks. The Shirley method was chosen for obtaining the background of spectra, and the Nb 3d spectra were fitted by the Gaussian–Lorentzian line function.

Metal dispersion on the samples was measured using CO pulse chemisorption (BELCAT-B; BEL Japan Inc.) with a stoichiometry factor of Pt:CO = 1:1. Pretreatment was done at 120 °C under H_2 flow (50 sccm) for 1 h. 10% CO gas balanced with He was used as the gas pulse, and the measurement was carried out at 50 °C. H_2 temperature-programmed reduction (H_2-TPR) of the as-prepared samples was performed using a Micromeritics BELCAT-B (BEL Japan Inc.) instrument with a thermal conductivity detector under a 3.9% H_2/Ar gas stream (50 mL/min), at a heating rate of 10 °C/min from 50 to 700 °C. Before the measurement was started, the fine-powder samples were treated in He (50 mL/min) at 450 °C for 1 h, followed by cooling at room temperature. The amount of H_2 consumed for the reduction was measured with a thermal conductivity detector (TCD) and quantified using ChemMaster data analysis software. For CO–TPD experiments, the samples were reduced at 200 °C for 30 min using 3.9% H_2/Ar at a flow rate of 30 mL/min. The samples were purged with He (30 mL/min) at the reduction temperature for 1 h. After cooling to room temperature, pulses (0.5 mL) of 10% CO/He were injected into a stream of He flowing through the samples until surface saturation was obtained. Then, the temperature was raised to 750 °C at the rate of 10 °C/min.

2.4 Evaluation of Catalyst Activity

The CO oxidation reaction was performed in a flow reactor, as described in previous works [24, 25]. The reactant gas composition contained CO and O_2 with He used as the carrier gas (He:CO:O_2 = 43:2:5), and the total gas flow rate was kept at 50 mL/min for all experiments which were controlled by mass flow controllers. Initially, 10 mg of the catalyst was diluted with 90 mg gamma-Al_2O_3 (97%) and then loaded into a tubular reactor. CO oxidation was carried out until 100% CO conversion was reached (at temperatures between 50 and 300 °C). Gas chromatography (DS Science) was used to analyze the mixed gas passing through the catalyst powder. The turnover frequency (TOF (s^{-1})) was determined based on the active Pt sites, which were measured using CO chemisorption [26]. In detail, the conversion of CO is kept below 20% to get the catalyst TOF value to ensure that the reaction is not affected by diffusion.

3 Results and Discussion

3.1 Characterization of the Synthesized Catalysts

Figure 1a displays the XRD patterns of a series of materials in the range of 10°–80°. Diffraction peaks corresponding to the crystal planes (111), (220), (311), (222), (400), (511), and (440) of γ-Al_2O_3 were observed at 19.4°, 31.9°, 37.5°, 39.3°, 45.7°, 60.5°, and 66.6°, respectively (PDF number:

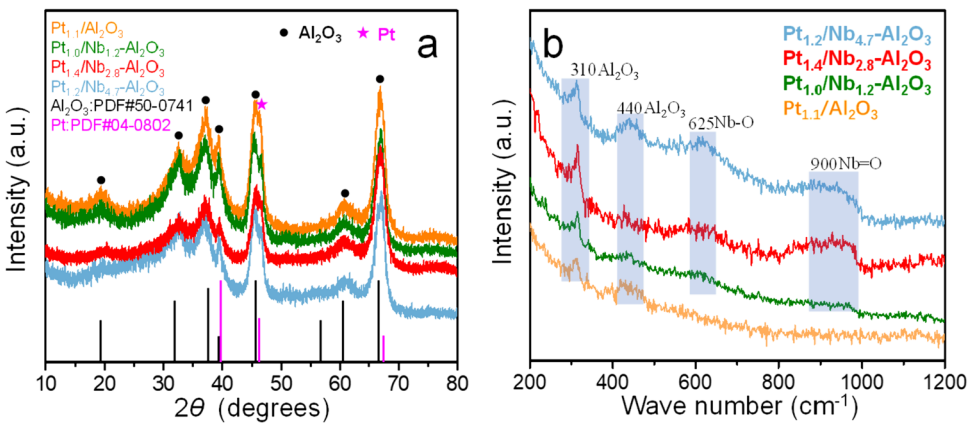

Fig. 1 **a** XRD patterns and **b** Raman spectra of Pt/Al_2O_3 and Nb-doped catalysts

50-0741) [27, 28]. For the Nb-doped Pt/Al_2O_3 materials, the same characteristic peaks were still present in the XRD patterns, indicating that the crystal structure of γ-Al_2O_3 remained unchanged after loading with metal oxides. Additionally, diffraction peaks at 46.2° were assigned to the (200) planes of Pt particles with a face-centered cubic (FCC) structure (PDF number: 04-0802) [29, 30]. Furthermore, no characteristic peaks corresponding to NbOx were detected in any of the patterns, possibly due to the uniform dispersion of Nb species on the alumina carrier surface or the low crystallinity and amorphous nature of Nb species [31–34]. Additionally, with an increase in the doping amount of Nb, a reduction in the intensity of the alumina characteristic peaks was observed, which might be attributed to the coverage of bulk NbO_x or interactions between the NbO_x species and the Al_2O_3 support [35, 36].

In order to further verify the structural features of the catalyst, we conducted a Raman test, and the results were shown in Fig. 1b. All samples had two obvious bands at 310 and 440 cm^{-1} assigned to bayerite or gibbsite from the Al_2O_3 support, respectively. Notably, the peak at 440 cm^{-1} exhibited a lower signal over the $Pt_{1.4}/Nb_{2.8}$–Al_2O_3 sample, possibly because an appropriate dispersion of niobium species weakened the characteristic peak of the Al_2O_3 support. No strong characteristic narrow peaks were observed in the Raman spectra of a series of alumina samples, mainly due to the low polarizability of light atoms and the ionic character of the Al–O bonds or the presence of the cubic crystal symmetry nature of γ-Al_2O_3 [37–39]. Moreover, broad bands between 600 and 650 cm^{-1} were assigned to the ν2 transverse optical modes of Nb–O stretching, whereas the modes around the 900 cm^{-1} regions were ascribed to the high concentration of terminal surface Nb=O groups [40, 41]. Hence, Raman spectra were consistent with the XRD results, confirming highly dispersed Pt species and Nb_2O_5 phase loaded on the surface of γ-Al_2O_3.

TEM microscopy image and the corresponding particle size distributions of $Pt_{1.1}/Al_2O_3$ and Pt/Nb–Al_2O_3 catalysts are shown in Fig. 2, and the elemental mapping of Pt and Nb are shown in Fig S1. It can be observed that the alumina catalyst exhibits a rod-shaped structure, with small dark spots

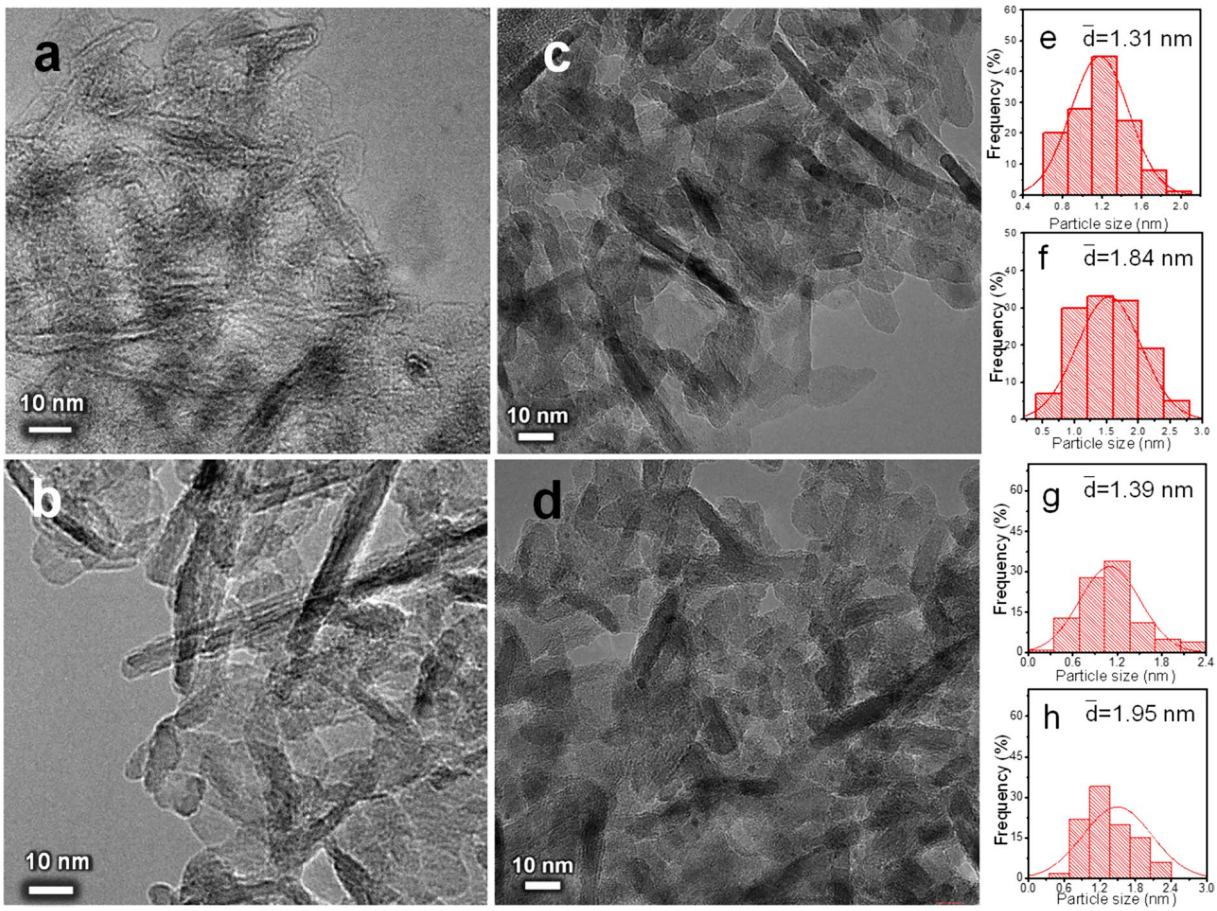

Fig. 2 TEM images of the synthesized: **a, e** $Pt_{1.1}/Al_2O_3$, **b, f** $Pt_{1.0}/Nb_{1.2}$–Al_2O_3, **c, g** $Pt_{1.4}/Nb_{2.8}$–Al_2O_3, and **d, h** $Pt_{1.2}/Nb_{4.7}$–Al_2O_3 catalysts and their corresponding particle size distributions

presumed to be Pt particles dispersed on the catalyst surface. The inset HR-TEM image of $Pt_{1.4}/Nb_{2.8}$–Al_2O_3 shows a random Pt nanoparticle with a lattice fringe of 0.230 nm, which is attributed to the Pt (111) surface [42, 43]. Both the TEM and EDS data ascertained the successful deposition of Pt NPs on the synthesized Nb-doped Al_2O_3 supports. Additionally, a homogeneous distribution of Al and Nb could also be observed across the entire mapped area from the EDS mapping, indicating the effective doping of Nb into the Al_2O_3. For the Nb-doped catalysts, Pt particles display relatively narrow distributions between 0.3 and 2.4 nm with the majority of particles at about 1.5 nm. The mean particle sizes of material Pt particles can be further counted based on surface area weighted diameter. The mean Pt particle size of $Pt_{1.4}/Nb_{2.8}$–Al_2O_3 was 1.39 nm, similar to the particle size of $Pt_{1.1}/Al_2O_3$ (1.31 nm) and smaller than that of $Pt_{1.2}/Nb_{4.7}$–Al_2O_3 (1.95 nm). Furthermore, the Nb elemental mapping image of $Pt_{1.2}/Nb_{4.7}$–Al_2O_3 is more obvious, and the Pt particle is rather vague in the TEM image compared with $Pt_{1.4}/Nb_{2.8}$–Al_2O_3, reflecting that excessive Nb content would influence the Pt dispersion.

Redox properties of the catalysts were measured by the H_2-TPR technique (Fig. 3a). The Al_2O_3 support does not show any distinct reduction peak in the temperature range of 50–700 °C, which agrees with the non-reducible nature of alumina [44, 45]. All catalysts show broad hydrogen uptake at 250 °C, the low-temperature reduction peak assigned to the reduction of weakly interacting Pt species, while a sharp contribution starts at a similar temperature of 200 °C. The subsequent flat peak that existed between 500 and 600 °C was attributed to Pt species strongly interacting with the support. These peaks shifted to lower temperatures with increasing Nb metal doping, which might be related to the smaller Pt particles, making the sample more reducible [46, 47]. The H_2 consumption determined by deconvolution of peaks followed the trend $Pt_{1.4}/Nb_{2.8}$–$Al_2O_3 < Pt_{1.2}/Nb_{4.7}$–$Al_2O_3 < Pt_{1.0}/Nb_{1.2}$–$Al_2O_3 < Pt_{1.1}/Al_2O_3$ (Table S1). These data suggest that Pt/Al_2O_3 had a slightly more oxidized Pt species than Pt/Nb–Al_2O_3, which consequently showed that Nb doping influenced the formation of oxidized Pt phases. The H_2-TPR results indicated that the Nb dopant significantly enhances the reducibility of the Pt catalysts, particularly in high-temperature regions.

Figure 3b shows the CO–TPD profile for the Pt-based catalysts, which could investigate CO species adsorption performance on the catalyst. There are two distinct CO desorption peaks for both the Nb-doped and non-doped samples when compared with the blank curve, which was obtained without CO gas. The initial peak is centered at low temperatures of 90 °C for Pt/Al_2O_3 and at 200 °C for Pt/Nb–Al_2O_3, which is attributed to the weakly adsorbed CO species. It was reported that these CO species are not active for CO oxidation, and they compete with O_2 to adsorb on the active sites in the low-temperature region, resulting in poor reactive oxygen species and low activity of the samples [48, 49]. Obviously, the weakly adsorbed CO peak of Pt/Nb–Al_2O_3 has a larger area and starts at a higher temperature than that of Pt/Al_2O_3, which indicates that there are more available active sites for both CO species and O_2 adsorbed on the Pt/Nb–Al_2O_3 catalysts. The second peak around 400–600 °C for all samples is assigned to the moderately adsorbed CO species on the catalysts [49–51]. Nb species might block Pt active sites for CO oxidation on Pt/Nb–Al_2O_3, leading to a slightly higher temperature shift when compared to non-doped Pt/Al_2O_3 catalysts for the high-temperature CO adsorption performance [52].

To further figure out the electronic interaction between Nb-doped Al_2O_3 support and Pt species, XPS was employed for the Pt-based catalysts, as shown in Fig. 4. In the Nb 3d regions (Fig. 4a), the peaks at binding energies 206.6 and 209.3 eV correspond to Nb^{4+} of $3d_{5/2}$ and $3d_{3/2}$ orbital with a spin–orbit splitting of 2.7 eV, whereas the other two peaks at 207.4 and 210.1 eV can be attributed to the $3d_{5/2}$ and $3d_{3/2}$ orbitals of Nb^{5+} [53–56]. The introduction of Nb into Pt/Al_2O_3 and the increase in Nb content for Pt/Nb–Al_2O_3 catalysts resulted in a positive shift in binding energy (the

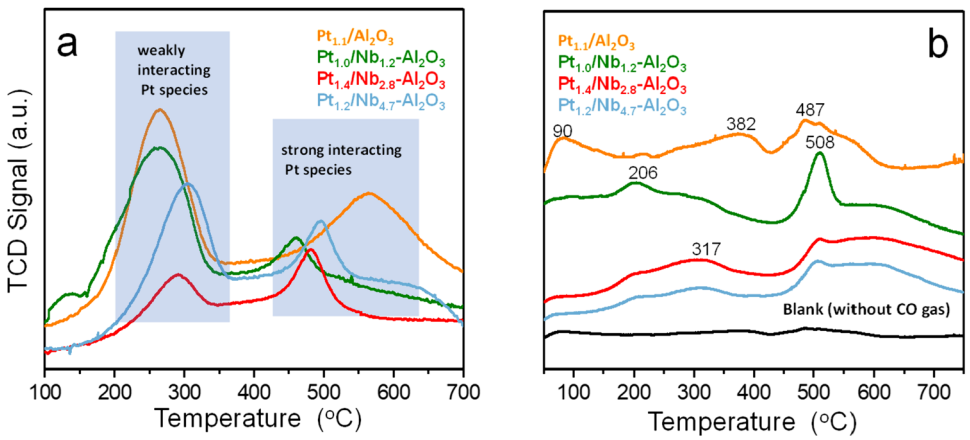

Fig. 3 **a** H_2-TPR profiles and **b** CO–TPD profiles of Pt/Al_2O_3 and Nb-doped catalysts

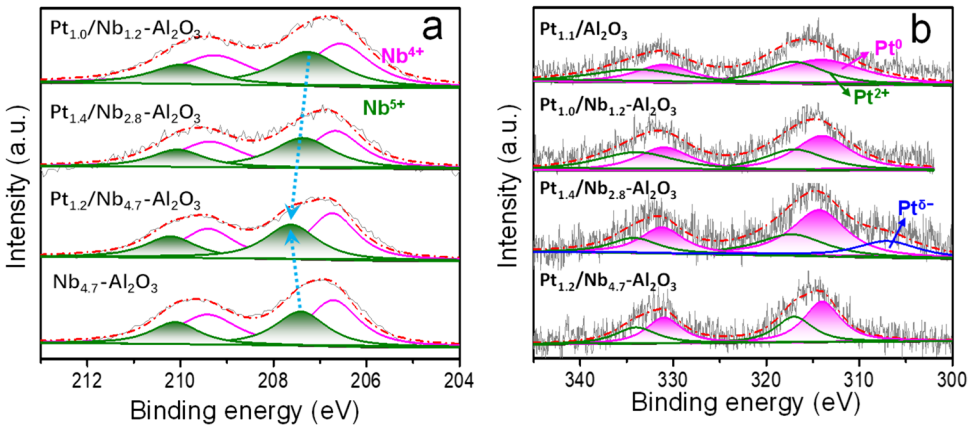

Fig. 4 XPS spectra of the Pt/Al_2O_3 and Pt/Nb–Al_2O_3 catalysts with different Nb contents in **a** the Nb 3d region, and **b** the Pt 4d region

raw data can be seen in Fig S2 and peak position details are shown in Table S2), indicating there was a strong interaction between Nb-doped Al_2O_3 support and Pt metal particles. Meanwhile, the Nb^{4+}/Nb^{5+} ratio (calculated based on the relative intensity of catalysts from the deconvolution of the XPS spectra) of $Pt_{1.2}/Nb_{4.7}$–Al_2O_3 (1.33) was lower than that of $Nb_{4.7}$–Al_2O_3 (1.50) and $Pt_{1.0}/Nb_{1.2}$–Al_2O_3 (1.39), which further clarified that there was electron transfer from Nb-doped support to Pt metal particles due to the strong metal support interaction [57, 58]. Because of the partial overlapping signal between Pt 4f and Al 2p in the alumina support with the Al Kα anode target, we used the Pt 4d signals to distinctly identify Pt species (Fig. 4b). The Pt $4d_{5/2}$ and Pt $4d_{3/2}$ peaks can both be deconvoluted into two spin–orbit doublets (the raw data and peak position details are shown in Fig S3 and Table S3), reflecting the dominant population of Pt^0 and the minor population of Pt^{2+}, while the Pt $4d_{5/2}$ peaks at 314.0 and 317.0 eV were attributed to Pt^0 and Pt^{2+}, respectively [59–61]. The binding energy of the Pt $4d_{5/2}$ state of Pt^0 was unaffected by the Nb addition when Pt/Al_2O_3 was compared with Pt/Nb–Al_2O_3, but the calculated ratio of Pt^0/Pt^{2+} showed a slightly increased trend after Nb doping (as shown in Table S4), which meant a higher electron density of Pt atoms [62, 63]. Additionally, $Pt_{1.4}/Nb_{2.8}$–Al_2O_3 exhibited another peak at 307 eV, accounting for the electron-rich platinum species ($Pt^{\delta-}$).

3.2 CO Oxidation Activity

The dependence of CO conversion on the reaction temperature for all the synthesized catalysts was depicted in Fig. S4. All catalysts exhibited comparable S-shaped conversion curves, wherein CO conversion augmented with elevated reaction temperatures. The experiments had very high repeatability with experimental errors of conversion rates below 10%, as confirmed by two separate runs of CO oxidation on the Pt/Al_2O_3 and Pt/NbOx–Al_2O_3 catalysts. The temperatures corresponding to 50% CO conversion (T_{50}) of Pt/Nb–Al_2O_3, Pt/Al_2O_3, Pt/V–Al_2O_3, Pt/Mo–Al_2O_3, and Pt/W–Al_2O_3 were 216 °C, 227 °C, 239 °C, 245 °C, and 251 °C, respectively. Notably, CO displayed a swift rise in high-temperature regions, particularly beyond 210 °C. To further distinguish the difference between catalysts, we also compared several conversion rates around 210 °C, and the results are shown in Fig. 5. Figure 5a distinctly illustrates the inhibitory activity of catalysts doped with metals other than Nb in CO catalytic oxidation, when compared to the niobium-doped catalyst. From 214 to 220 °C, the conversion rate of Pt/Nb–Al_2O_3 rapidly escalated from 21.63 to 97.61%, while other catalysts exhibited only marginal increases in conversion rate. Between 220 and 225 °C, the conversion rate of Pt/Al_2O_3 exhibited rapid growth, whereas catalysts modified with other metals continued to display sluggish growth. To clarify the distinctions in catalytic reactions among various catalysts, H_2-TPR was conducted as shown in Fig. S5a. The Nb-doped samples have similar reduction properties compared to their Nb-free counterpart, but a distinct difference is observed between other M-doped and non-doped catalysts. As for Pt/Mo–Al_2O_3 and Pt/W–Al_2O_3, the hydrogen consumption uptake is over 600 °C, mainly due to the evolution of new surface species, which could hardly be reduced because of the metal doping. Thus, it was speculated that the altered reducibility of the materials might be responsible for the poor catalytic activity of Pt/Mo–Al_2O_3 and Pt/W–Al_2O_3. For Pt/V–Al_2O_3, which maintained or even improved its reduction property, XPS was employed for further characterization, as depicted in Fig. S5b. Comparative analysis of Pt^0/Pt^{2+} ratios between Pt/Nb–Al_2O_3 (1.48), Pt/V–Al_2O_3 (1.19), and Pt/Al_2O_3 (1.39) revealed that niobium doping enhanced the proportion of Pt^0, whereas vanadium doping increased the proportion of Pt^{2+}. Considering the catalytic activity outcomes and XPS analysis, implying that the electron effects between Pt and Nb species showed a conductive impact on CO catalytic oxidation [64, 65].

Figure 5b presents a comparison of CO conversion rates among catalysts with varying amounts of Nb doping

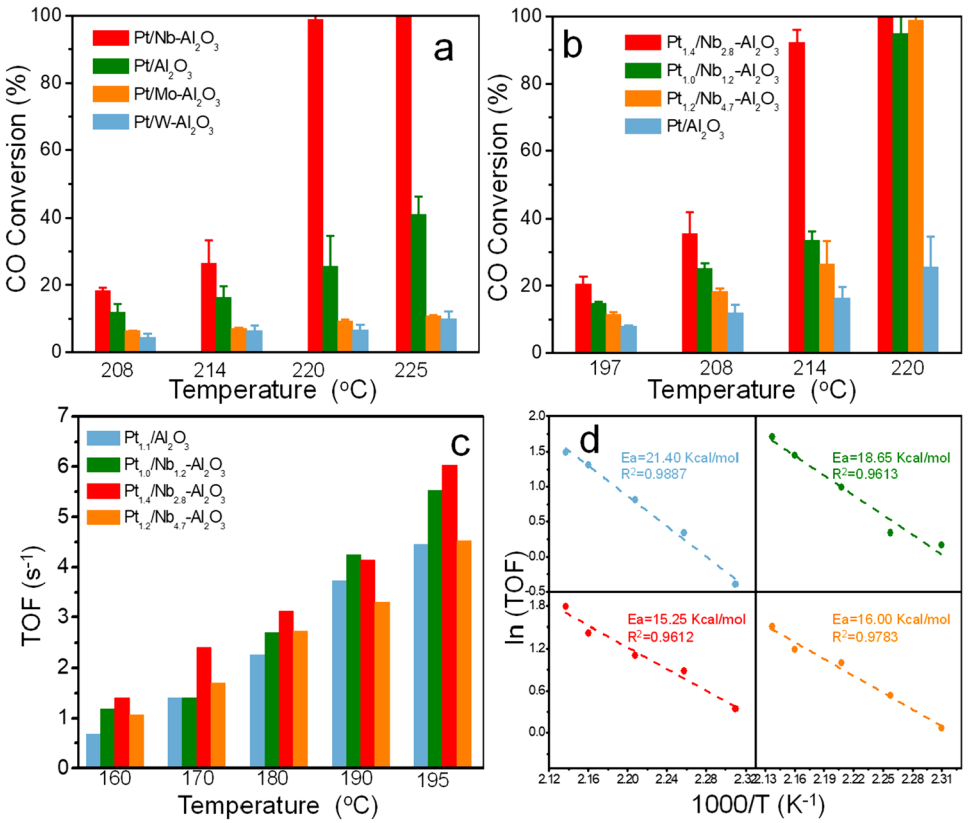

Fig. 5 CO conversion at different reaction temperatures for **a** different metal oxide doped Pt/Al_2O_3 catalysts and **b** Nb-doped Pt/Al_2O_3 catalysts with different Nb content, **c** TOF calculated at different reaction temperatures and **d** Arrhenius plot of the Pt/Al_2O_3 and Pt/Nb–Al_2O_3 catalysts

(corresponding CO conversion as a function of temperature over Pt/Nb–Al_2O_3 with different Nb content is displayed in Fig.S3b). The activity sequence of Nb-doped Pt/Al_2O_3 catalysts was as follows: $Pt_{1.4}/Nb_{2.8}$–Al_2O_3 > $Pt_{1.0}/Nb_{1.2}$–Al_2O_3 > $Pt_{1.2}/Nb_{4.7}$–Al_2O_3. Catalytic activity improved while the Nb content increased from 1.20 to 2.84 wt%, as evidenced by a decrease in T_{50} from 215 °C to 210 °C. However, further escalation of Nb content leads to decreased activity, with T_{50} increasing once again. TEM and XPS analyses reveal that excessive Nb doping affects both Pt dispersion and the proportion of metallic platinum species. Consequently, CO oxidation activity diminishes. $Pt_{1.4}/Nb_{2.8}$–Al_2O_3 demonstrated optimal catalytic performance, which might be related to electron transfer and Pt/NbOx interface, underscoring the significance of the electron effect between Pt and Nb species in influencing CO oxidation activity. After CO oxidation reaction, Pt NPs in $Pt_{1.4}/Nb_{2.8}$–Al_2O_3 retained a size similar to the initial state (1.40 nm), showing the absence of sintering (Fig. S6). This indicates the stability of the catalyst in high-temperature oxidation reactions, highlighting the performance enhancement attributed to Nb doping.

Figure 5c shows TOFs calculated at different reaction temperatures. The TOF of Pt/Nb–Al_2O_3 at four temperatures always exhibited a similar trend with conversion rate: $Pt_{1.4}/Nb_{2.8}$–Al_2O_3 > $Pt_{1.0}/Nb_{1.2}$–Al_2O_3 > $Pt_{1.2}/Nb_{4.7}$–Al_2O_3.

Figure 5d illustrates Arrhenius plots of ln (TOF) versus 1000/T for $Pt_{1.1}/Al_2O_3$ and Pt/Nb–Al_2O_3 catalysts. Table 1 provides details on the catalysts' TOFs at 180 °C and the calculated activation energies (Ea) based on the Arrhenius equation. Variations in TOF values align with the trends observed in reaction rates, with $Pt_{1.4}/Nb_{2.8}$–Al_2O_3 exhibiting a higher TOF value of 3.12 s^{-1} and a lower Ea of 15.25 kcal/mol than other catalysts.

4 Conclusion

In this study, Pt-based catalysts doped with varying Nb contents were synthesized to investigate the influence of doping of niobium oxide on the catalytic activity of Pt/Al_2O_3 for CO oxidation. The influence of Nb doping on the structure and surface chemical composition of Pt/Al_2O_3 and Pt/Nb–Al_2O_3 catalysts was explored through systematic characterization. Combined XRD, Raman, and XPS analyses confirmed that Nb doping had no impact on the structure of alumina but significantly induced electron effect and the interface between Pt and Nb phase. Niobium doping promoted platinum reduction, leading to an increase in metallic platinum content, attributed to strong metal–support interactions between Pt and Nb-doped Al_2O_3 carriers. TEM and CO adsorption results also demonstrated that niobium

doping favored platinum dispersion. In the catalytic CO oxidation reaction, Pt/Nb–Al_2O_3 was relatively dominant when compared with other metal-doped catalysts, owing to the more stable reducibility according to the H_2-TPR results. Additionally, the CO–TPD showed the special CO adsorbed properties for Nb-doped catalysts which supplied more possibilities for oxygen adsorption in the low-temperature zone. Pt/Nb–Al_2O_3 catalyst with different Nb content exhibited a promoting effect relative to Pt/Al_2O_3, while $Pt_{1.4}/Nb_{2.8}$–Al_2O_3 also showed a superior T_{50} of 200 °C and TOF of 3.12 s^{-1} at 180 °C than $Pt_{1.2}/Nb_{4.7}$–Al_2O_3 catalyst with excessive Nb content. This finding emphasizes the potential of niobium oxide doping to enhance the catalytic activity of Pt-based catalysts for CO oxidation, offering new opportunities for optimizing catalytic processes in the field.

Supplementary Information The online version contains supplementary material available at https://doi.org/10.1007/s11244-024-01924-w.

Acknowledgements This work is supported by the National Research Foundation of Korea (NRF) grant funded by the Korean government (MSIT) (2022R1A2C3004242).

Funding Open Access funding enabled and organized by KAIST.

Data availability The authors confirm that the data supporting the findings of this study are available within the article and/or its supplementary materials.

References

1. Venkataswamy P, Jampaiah D, Mukherjee D, Aniz CU, Reddy BM (2016) Mn-doped ceria solid solutions for CO oxidation at lower temperatures. Catal Lett 146(10):2105–2118
2. Dey S, Dhal GC, Mohan D, Prasad R (2019) Ambient temperature complete oxidation of carbon monoxide using hopcalite catalysts for fire escape mask applications. Adv Compos Hybrid Mater 2(3):501–519
3. Al Soubaihi R, Saoud K, Dutta J (2018) Critical review of low-temperature CO oxidation and hysteresis phenomenon on heterogeneous catalysts. Catalysts 8(12):660
4. Haneda M, Watanabe T, Kamiuchi N, Ozawa M (2013) Effect of platinum dispersion on the catalytic activity of Pt/Al_2O_3 for the oxidation of carbon monoxide and propene. Appl Catal B 142–143:8–14
5. Cha BJ, Kim SY, Choi CM, Sung JY, Choi MC, Seo HO, Kim YD (2021) Ultra-low loading of iron oxide on Pt/Al_2O_3 for enhanced catalytic activity of CO oxidation at room temperature: A simple method for applications. Chem Eng J 404(15):12560
6. Gibson EK, Crabb EM, Gianolio D, Russell AE, Thompsett D, Wells PP (2017) Understanding the role of promoters in catalysis: Operando XAFS/DRIFTS study of CeOx/Pt/Al_2O_3 during CO oxidation. Catal Struct React 3(1–2):5–12
7. An N, Yuan X, Pan B, Li Q, Li S, Zhang W (2014) Design of a highly active Pt/Al_2O_3 catalyst for low-temperature CO oxidation. RSC Adv 4(72):38250–38257
8. Choi H, Lee J, Kim D, Kumar A, Jeong B, Kim K-J, Lee H, Park JY (2021) Influence of lattice oxygen on the catalytic activity of blue titania supported Pt catalyst for CO oxidation. Catal Sci Technol 11(5):1698–1708
9. Song HC, Oh S, Kim SH, Lee SW, Moon SY, Choi H, Kim S-H, Kim Y, Oh J, Park JY (2019) The effect of the oxidation states of supported oxides on catalytic activity: CO oxidation studies on Pt/cobalt oxide. Chem Commun 55(64):9503–9506
10. Bosio N, Di M, Skoglundh M, Carlsson P-A, Grönbeck H (2022) Interface reactions dominate low-temperature CO oxidation activity over Pt/CeO2. J Phys Chem C 126(38):16164–16171
11. McClure SM, Goodman DW (2009) New insights into catalytic CO oxidation on Pt-group metals at elevated pressures. Chem Phys Lett 469(1–3):1–13
12. Ganzler AM, Casapu M, Doronkin DE, Maurer F, Lott P, Glatzel P, Votsmeier M, Deutschmann O, Grunwaldt JD (2019) Unravelling the different reaction pathways for low temperature CO oxidation on Pt/CeO_2 and Pt/Al_2O_3 by spatially resolved structure-activity correlations. J Phys Chem Lett 10(24):7698–7705
13. Shin K, Zhang L, An H, Ha H, Yoo M, Lee HM, Henkelman G, Kim HY (2017) Interface engineering for a rational design of poison-free bimetallic CO oxidation catalysts. Nanoscale 9(16):5244–5253
14. Oh S, Ha H, Choi H, Jo C, Cho J, Choi H, Ryoo R, Kim HY, Park JY (2020) Oxygen activation on the interface between Pt nanoparticles and mesoporous defective TiO_2 during CO oxidation. J Chem Phys 151(23):234716
15. van Deelen TW, Hernández Mejía C, de Jong KP (2019) Control of metal-support interactions in heterogeneous catalysts to enhance activity and selectivity. Nat Catal 2(11):955–970
16. Kim J, Choi H, Kim D, Park JY (2021) Operando surface studies on metal-oxide interfaces of bimetal and mixed catalysts. ACS Catal 11(14):8645–8677
17. Song S, Wu Y, Ge S, Wang L, Wang Y, Guo Y, Zhan W, Guo Y (2019) A facile way to improve Pt atom efficiency for CO oxidation at low temperature: modification by transition metal oxides. ACS Catal 9(7):6177–6187
18. Trung Tran SB, Choi HS, Oh SY, Moon SY, Park JY (2018) Iron-doped ZnO as a support for Pt-based catalysts to improve activity and stability: enhancement of metal-support interaction by the doping effect. RSC Adv 8(38):21528–21533
19. Nowak I, Ziolek M (1999) Niobium compounds: preparation, characterization, and application in heterogeneous catalysis. Chem Rev 99:3603–3624
20. Park D, Kim SM, Kim SH, Yun JY, Park JY (2014) Support effect on the catalytic activity of two-dimensional Pt nanoparticle arrays on oxide substrates. Appl Catal A 480:25–33
21. Tran SBT, Choi H, Oh S, Park JY (2019) Defective Nb_2O_5-supported Pt catalysts for CO oxidation: promoting catalytic activity via oxygen vacancy engineering. J Catal 375:124–134
22. Zhang J, Wang L, Hu X, Shao Q, Xu X, Long C (2021) Balancing surface acidity, oxygen vacancies and Cu^+ of CuO_x/CeO_2 catalysts by Nb doping for enhancing CO oxidation and moisture resistance and lowering byproducts in plasma catalysis. J Clean Prod 318(10):128564

23. Jardim EO, Rico-Francés S, Coloma F, Anderson JA, Ramos-Fernandez EV, Silvestre-Albero J, Sepúlveda-Escribano A (2015) Preferential oxidation of CO in excess of H_2 on Pt/CeO_2–Nb_2O_5 catalysts. Appl Catal A 492:201–211
24. Yoo M, Kang E, Choi H, Ha H, Choi H, Choi J-S, Lee K-S, Celestre R, Shapiro DA, Park JY, Kim C, Yu Y-S, Kim HY (2022) Enhancing the inherent catalytic activity and stability of TiO_2 supported Pt single-atoms at CeOx–TiO_2 interfaces. J Mater Chem A 10(11):5942–5952
25. Jung C-H, Yun JC, Qadir K, Naik B, Yun JY, Park JY (2014) Catalytic activity of Pt/SiO_2 nanocatalysts synthesized via ultrasonic spray pyrolysis process under CO oxidation. Appl Catal B 154:171–176
26. Aramendia MA, Borau V, Jimnez C, Marinas JM, Moreno A (1996) Comparative measurements of the dispersion of Pd catalyst on SiO_2-A1PO_4 support using TEM and H_2 chemisorption. Colloids Surf A 106:161–165
27. Jiao H, Zhao X, Lv C, Wang Y, Yang D, Li Z, Yao X (2016) Nb_2O_5-gamma-Al_2O_3 nanofibers as heterogeneous catalysts for efficient conversion of glucose to 5-hydroxymethylfurfural. Sci Rep 6:34068
28. Sararuk C, Yang D, Zhang G, Li C, Zhang S (2018) A simple strategy to synthesize and characterization of zirconium modified PCs/γ–Al_2O_3. Chin J Chem Eng 26(5):1209–1212
29. Li M, Hu Y, Fu HY, Qu X, Xu Z, Zheng S (2019) Pt embedded in carbon rods of N-doped CMK-3 as a highly active and stable catalyst for catalytic hydrogenation reduction of bromate. Chem Commun 78(55):11786–11789
30. Li M, Li W, Yang Y, Yu D, Lin J, Wan R, Zhu H (2023) Remarkably efficient Pt/CeO_2–Al_2O_3 catalyst for catalytic hydrodeiodination of monoiodoacetic acid: synergistic effect of Al_2O_3 and CeO_2. Chemosphere 327:138515
31. Francisco MSP, Gushikem Y (2002) Synthesis and characterization of SiO_2-Nb_2O_5 systems prepared by the sol-gel method: structural stability studies. J Mater Chem 12(8):2552–2558
32. Zhang Y, Sun W, Rui X, Li B, Tan HT, Guo G, Madhavi S, Zong Y, Yan Q (2015) One-pot synthesis of tunable crystalline Ni_3S_4@amorphous MoS_2 core/shell nanospheres for high-performance supercapacitors. Small 11(30):3694–3702
33. Gallagher JR, Li T, Zhao H, Liu J, Lei Y, Zhang X, Ren Y, Elam JW, Meyer RJ, Winans RE, Miller JT (2014) In situ diffraction of highly dispersed supported platinum nanoparticles. Catal Sci Technol 4(9):3053–3063
34. Li C, Shao Z, Pang M, Williams CT, Liang C (2012) Carbon nanotubes supported Pt catalysts for phenylacetylene hydrogenation: effects of oxygen containing surface groups on Pt dispersion and catalytic performance. Catal Today 186(1):69–75
35. Li S, Yu X, Dang X, Meng X, Zhang Y, Qin C (2021) Non-thermal plasma coupled with MOx/γ-Al2O3 (M: Fe Co, Mn, Ce) for chlorobenzene degradation: analysis of byproducts and the reaction mechanism. J Environ Chem Eng 9(6):106562
36. Cao P, Zhang Y, Song F, Zhao H, Heng Pang C, Wu T (2022) Mn doped CeO_2-MoO_3/γ-Al_2O_3 catalysts for the enhanced adsorption and catalytic oxidation of Hg0 in oxygen atmosphere. Appl Surf Sci 581(15):152327
37. Radi PA, Testoni GE, Pessoa RS, Maciel HS, Rocha LA, Vieira L (2018) Tribocorrosion behavior of TiO_2/Al_2O_3 nanolaminate, Al_2O_3, and TiO_2 thin films produced by atomic layer deposition. Surf Coat Technol 349:1077–1082
38. Koichumanova K, Sai SankarGupta KB, Lefferts L, Mojet BL, Seshan K (2015) An in situ ATR-IR spectroscopy study of aluminas under aqueous phase reforming conditions. Phys Chem Chem Phys 17(37):23795–23804
39. Gangwar J, Gupta BK, Tripathi SK, Srivastava AK (2015) Phase dependent thermal and spectroscopic responses of Al_2O_3 nanostructures with different morphogenesis. Nanoscale 7(32):13313–13344
40. Crivelaro VM, Cortez GG (2023) Propane oxidative dehydrogenation over Sr-doped V catalyst supported on Nb_2O_5-Al_2O_3. Catal Lett 153:3651–3664
41. Nascimento JPS, Oton LF, Oliveira AC, Rodríguez-Aguado E, Rodríguez-Castellón E, Araujo RS, Souza MS, Lang R (2020) Selective catalytic reduction of NOx by CO over doubly promoted MeMo/Nb_2O_5 catalysts (Me = Pt, Ni, or Co). Catalysts 10(9):1048
42. Huang L-L, Xu L-L, Gao B-W, Ma Y-K, Jia A-P, Wang Y, Lu J-Q (2023) Deep oxidation of propane over PtIr/TiO_2 bimetallic catalysts: mechanistic investigation of promoting roles of Ir species. Appl Surf Sci 638(30):158149
43. Xu H, Song P, Yan B, Wang J, Wang C, Shiraishi Y, Yang P, Du Y (2018) Pt islands on 3 D nut-like PtAg nanocrystals for efficient formic acid oxidation electrocatalysis. ChemSusChem 11(6):1056–1062
44. Araiza DG, González-Vigi F, Gómez-Cortés A, Arenas-Alatorre J, Díaz G (2021) Pt-based catalysts in the dry reforming of methane: effect of support and metal precursor on the catalytic stability. J Mex Chem Soc 65(1):1262
45. Melchor-Hernández C, Gómez-Cortés A, Díaz G (2013) Hydrogen production by steam reforming of ethanol over nickel supported on La-modified alumina catalysts prepared by sol-gel. Fuel 107:828–835
46. Wang Y, Liu H-H, Wang S-Y, Luo M-F, Lu J-Q (2014) Remarkable enhancement of dichloromethane oxidation over potassium-promoted Pt/Al_2O_3 catalysts. J Catal 311:314–324
47. Bhogeswararao S, Srinivas D (2015) Catalytic conversion of furfural to industrial chemicals over supported Pt and Pd catalysts. J Catal 327:65–77
48. Ahasan MR, Wang Y, Wang R (2022) In situ DRIFTS and CO-TPD studies of CeO_2 and SiO_2 supported CuOx catalysts for CO oxidation. Mol Catal 518:112085
49. Zhou Y, Wang Z, Liu C (2015) Perspective on CO oxidation over Pd-based catalysts. Catal Sci Technol 5(1):69–81
50. Zhang N, Li L, Wu R, Song L, Zheng L, Zhang G, He H (2019) Activity enhancement of Pt/MnOx catalyst by novel β-MnO_2 for low-temperature CO oxidation: study of the CO-O_2 competitive adsorption and active oxygen species. Catal Sci Technol 9(2):347–354
51. Xu J-D, Chang Z-Y, Zhu K-T, Weng X-F, Weng W-Z, Zheng Y-P, Huang C-J, Wan H-L (2016) Effect of sulfur on α-Al_2O_3-supported iron catalyst for Fischer-Tropsch synthesis. Appl Catal A 514:103–113
52. Mozer TS, Passos FB (2011) Selective CO oxidation on Cu promoted Pt/Al_2O_3 and Pt/Nb_2O_5 catalysts. Int J Hydrogen Energy 36(21):13369–13378
53. Gao Y, Qi L, He F, Xue Y, Li Y (2022) Selectively growing a highly active interface of mixed Nb-Rh oxide/2D carbon for electrocatalytic hydrogen production. Adv Sci 9(10):2104706
54. Alov NV (2007) Surface oxidation of metals by oxygen ion bombardment. Nucl Instrum Methods Phys Res B 256(1):337–340
55. Park N, Kim YT, Park Y, Cho JY, Oh SS, Heo J, Son J (2020) Voltage-triggered insulator-to-metal transition of ALD NbOx thin films for a two-terminal threshold switch. J Mater Chem C 8(41):14365–14369
56. Li S, Schmidt CN, Xu Q, Cao X, Cao G (2016) Macroporous nanostructured Nb_2O_5 with surface Nb4+ for enhanced lithium ion storage properties. ChemNanoMat 2(7):675–680
57. Su H, Huang Y-T, Chang Y-H, Zhai P, Hau NY, Cheung PCH, Yeh W-T, Wei T-C, Feng S-P (2015) The synthesis of Nb-doped TiO_2 nanoparticles for improved-performance dye sensitized solar cells. Electrochim Acta 182:230–237

58. Jimenez-Morales I, Cavaliere S, Jones D, Roziere J (2018) Strong metal-support interaction improves activity and stability of Pt electrocatalysts on doped metal oxides. Phys Chem Chem Phys 20(13):8765–8772
59. Bai S, Huang B, Shao Q, Huang X (2018) Universal strategy for ultrathin Pt-M (M = Fe Co, Ni) nanowires for efficient catalytic hydrogen generation. ACS Appl Mater Interfaces 10(26):22257–22263
60. Resende NS, Perez CA, Eon JG, Schmal M (2011) The effect of coating TiO_2 on the CO oxidation of the Pt/γ-Alumina catalysts. Catal Lett 141(11):1685–1692
61. Meng F, Yang X, Zhao S, Li Z, Zhang G, Qi Y, Chu S, Wang G, Zhang J, Qin Y, Zhang B (2023) Shifting reaction path for levulinic acid aqueous-phase hydrogenation by Pt-TiO_2 metal-support interaction. Appl Catal B 324:122236
62. Lin L-Y, Kavadiya S, He X, Wang W-N, Karakocak BB, Lin Y-C, Berezin MY, Biswas P (2020) Engineering stable Pt nanoparticles and oxygen vacancies on defective TiO_2 via introducing strong electronic metal-support interaction for efficient CO_2 photoreduction. Chem Eng J 389:123450
63. Cho SH, Park JS, Choi SH, Lee SK, Kim SH (2005) Effect of water vapor on carbon monoxide oxidation over promoted platinum catalysts. Catal Lett 103(3–4):257–261
64. Kim SB, Shin JH, Kim GJ, Hong SC (2022) Promoting metal-support interaction on Pt/TiO_2 catalyst by antimony for enhanced carbon monoxide oxidation activity at room temperature. Ind Eng Chem Res 61:14793–14803
65. He K, Wang Q (2021) Activation of Pt nanoclusters on TiO_2 via tuning the metallic sites to promote low-temperature CO oxidation. Catalysts 11:1280